



Global atmospheric chemistry: Integrating over fractional cloud cover

Jessica L. Neu,¹ Michael J. Prather,¹ and Joyce E. Penner²

Received 7 September 2006; revised 17 January 2007; accepted 28 February 2007; published 9 June 2007.

[1] A new approach defined here allows for the averaging of photochemistry over complex cloud fields within a grid square and can be readily implemented in current global models. As diagnosed from observations or meteorological models, fractional cloud cover with many overlying cloud layers can generate hundreds to thousands of different cloud profiles per grid square. We define a quadrature-based method, applied here to the problem of averaging photolysis rates over this range of cloud patterns, which opens new opportunities for modeling in-cloud chemistry in global models. We select up to four representative cloud profiles, optimizing the selection and weighting of each to minimize the difference in photolysis rates when compared with the integration over the entire set of cloud distributions. To implement our algorithm, we adapt the UCI fast-JX photolysis code to the cloud statistics from the ECMWF forecast model at T42L40 resolution. For the tropics and midlatitudes, grid-square-averaged photolysis rates for O₃, NO₂, and NO₃ using four representative atmospheres differ by at most 3.2% RMS from rates averaged over the hundreds or more cloudy atmospheres derived from a maximum-random overlap scheme. Further, bias errors in both the free troposphere and the boundary layer are less than 1%. Similar errors are shown to be 10–20% for current approximation methods. Errors in the quadrature method are less than the uncertainty in the choice of maximum-random overlap schemes. We apply the method to the averaging of photochemistry over different cloud profiles and outline extensions to heterogeneous cloud chemistry.

Citation: Neu, J. L., M. J. Prather, and J. E. Penner (2007), Global atmospheric chemistry: Integrating over fractional cloud cover, *J. Geophys. Res.*, 112, D11306, doi:10.1029/2006JD008007.

1. Introduction

[2] Accurate representation of the interaction between clouds and chemistry is a major challenge in atmospheric modeling. When integrating chemical rates over the atmosphere, one must include not only the mixed phase chemistry of cloudy regions, where heterogeneous reactions may dominate over those in the gas phase, but also the wide range in photochemical activity that results from various cloud fields. In a cloud-free atmosphere, for example, daytime photolysis rates remain high down to the ground. Above optically thick cloud decks, and even within the upper part of these clouds, photolysis rates can be twice as large as the corresponding clear-sky rates. Below optically thin clouds, photolysis rates are likewise enhanced, but in the lower part of thick clouds and beneath them, photolysis rates can be reduced several fold [e.g., Chang *et al.*, 1987; Madronich, 1987; Trautmann *et al.*, 1999; Wild *et al.*, 2000; Tie *et al.*, 2003; Kylling *et al.*, 2005].

[3] Superimposing satellite images of clouds on the grid of most global climate or chemistry models makes it clear

that cloud cover in these models needs to be quantified in terms of the fractional area occupied by clouds (cloud-fraction) in each atmospheric layer. Chemistry-transport models (CTMs) rely on atmospheric general circulation, climate, or assimilation models to generate cloud statistics, whether the CTMs are embedded in the circulation model or run off-line from archived meteorological fields. Cloud cover in a model level is generally diagnosed as the amount of water in liquid/solid phase and the cloud fractional area (CF, from 0 to 100% of the grid square), and the cloud algorithms are tested with observations [e.g., Weare, 1999; Palm *et al.*, 2005]. The ability to implement fractional cloud cover in CTMs avoids large, systematic errors introduced by distributing the amount of cloud uniformly over the grid square (i.e., reduced heating and photolysis rates below the cloud; and increased, above). This paper presents an innovative, accurate, and yet computationally efficient approach for implementing fractional cloud cover in a CTM.

[4] Specification of cloud optical properties and cloud-fraction in each layer is not sufficient to calculate the radiative transfer (e.g., heating and photolysis rates) without knowledge of how these cloud layers overlap. The required three-dimensional knowledge of the cloud distributions cannot be simply derived from nadir satellite images, and considerable research focuses on cloud observations and on how to best represent cloud fields in atmospheric models [Faure *et al.*, 2001; Lewis *et al.*, 2004; Brooks *et al.*, 2005;

¹Department of Earth System Science, University of California, Irvine, California, USA.

²Department of Atmospheric, Oceanic, and Space Sciences, University of Michigan, Ann Arbor, Michigan, USA.

Cornet et al., 2005; Gordon et al., 2005; Willen et al., 2005]. These models generally define the vertical distribution of clouds using either the random overlap or the maximum-random overlap scheme [e.g., Collins, 2001]. In random overlap, all clouds randomly overlap with all other clouds, while in maximum-random overlap, clouds within a group (defined in various ways) are maximally overlapped, while the groups themselves randomly overlap each other. Heating rates are then calculated as averages over some or all of the possible realizations of the vertical cloud distribution using precalculated reflection and transmission factors for each layer.

[5] Photochemistry requires a detailed solution of the equation of radiative transfer. Spectral resolution in the ultraviolet and visible, as well as the angular distribution of scattered light, is needed to calculate photolysis frequencies (J-values). This solution requires not only the vertical distribution of absorbers (ozone and some aerosols) and scatterers (aerosols and clouds) but also their complete optical properties, including the scattering phase function. The cost of calculating J-values in a CTM with realistic clouds and aerosols was prohibitive before the fast-J approach to multiple scattering and spectral bin optimization [Wild et al., 2000]. Even with fast-J or the equivalent Fast-TUV [Tie et al., 2003], most CTMs are still limited to calculating the J-values for one “average” atmosphere per grid box, which is generated either by averaging the clouds over the grid square [e.g., Wild et al., 2003; Bey et al., 2001], or approximating the random overlap of cloud layers as a single atmosphere [Briegleb, 1992].

[6] One early method of representing the effect of clouds on J-values [Logan et al., 1981; Spivakovsky et al., 2000] treated clouds as fully reflecting surfaces at different altitudes as in the work by London [1952] and averaged the J-values calculated for different cloud profiles. Another method [Chang et al., 1987] provided a scaling factor for J-values that depended on the vertically averaged cloud cover and the optical depth of clouds above. Broadband approaches were introduced [Landgraf and Crutzen, 1998], but they had large errors with thick cloud/aerosol layers and low sun angles. Tie et al. [2003] invoked a subgrid method for fractional cloud cover with Fast-TUV, but required all clouds in a maximally overlapping group to have a single cloud fraction, and did not test these results against the full set of cloud profiles.

[7] Feng et al. [2004] tested the impact of different subgrid cloud overlap schemes on global atmospheric chemistry. They compared CTM simulations using (1) an approximation for random overlap, (2) maximum-random overlap, and (3) the simple assumption of cloud averaging used in many CTMs [e.g., Wild et al., 2003]. Feng et al. [2004] conclude that both overlap schemes provide reasonable J-values and tropospheric hydroxyl radical (OH) abundances; whereas the uniform opacity in cloud averaging has large bias errors, i.e., lower OH abundances and hence a longer lifetime for CH₄. Their CTM relied on photolysis rate look-up tables because the number of radiative transfer calculations required for these cloud overlap schemes was computationally prohibitive. Here, we define a sampling methodology and quadrature method to make this problem tractable.

[8] Observations of clouds, from the ground, airplanes, or satellites, show a wide range of cloud distributions through-

out the troposphere. Despite this apparent continuum of vertical cloud profiles, there tend to be a few representative patterns of cloud cover in many regions, e.g., tropical cirrus decks often overlie convective cumulus and extend over adjacent clear regions. The concept of representative patterns inspires the approach taken here. We propose that the integration of photochemistry over a near continuum of different subgrid cloud distributions can be achieved by quadrature: that is, (1) selecting a few representative realizations of the vertical cloud profile by suitable sampling of all of the possibilities within a model grid, (2) computing the weighting (fractional area) for each representative realization based on the frequency of similar cloud distributions, (3) calculating the photochemistry only for each representative atmosphere, and (4) combining the weighted representative atmospheres to approximate the integral over all of the cloud profiles within the model grid.

[9] In section 2, we describe common approaches for defining the vertical overlap of fractional cloud cover and thus generating a set of cloud profiles for the radiative transfer computations. Our new quadrature-based algorithm for calculating average J-values is presented in section 3. Updates to the UCI fast-JX photolysis code [Wild et al., 2000; Bian and Prather, 2002] are described in section 4. The accuracy of the new algorithm is evaluated in section 5 using fast-JX and a 24-hour period of cloud diagnostics from the Oslo-derived ECMWF pieced forecast meteorological fields [Wild et al., 2003]. We compare average J-values calculated from the complete set of cloud profiles in each grid square, numbering in the hundreds to thousands, with those calculated using our quadrature method with four representative cloud profiles. In section 6, we conclude with a brief look at how treatment of fractional cloud cover might impact the shortwave albedo and tropospheric ozone chemistry. In the latter case we look at the next step in CTM development: averaging the separate photochemistry occurring in each column atmosphere, rather than calculating a single photochemistry with the average of in-cloud and clear-sky rates.

2. Treatment of Overlapping Clouds and Radiative Transfer

[10] Given a profile of CF for a grid square, a scheme for treating vertical cloud overlap must be chosen. The scheme is used to generate a set of cloud profiles to represent the grid square, each profile having either 0 or 100% cloud fraction in each vertical level. We assume that the photochemistry of the whole grid square can be treated linearly and can thus be calculated as the integral over these cloud profiles. The radiative transfer solution used here further assumes that each profile can be treated as an independent column atmosphere (ICA).

[11] As an example of fractional cloud cover, Figure 1 shows an idealized grid square from an 8-layer model with 2 cloud groups: cirrus-like cloud layers with large cloud fraction (CF) and small optical depths (OD) in layers 6 and 7; and stratus-like cloud layers with smaller CF and larger OD in layers 3 and 4. The simplest approximation, denoted here as AVG, is simply to spread the cloud uniformly over the entire grid square, thus reducing its optical depth, $OD_{AVG} = OD \times CF$. This produces thinner clouds

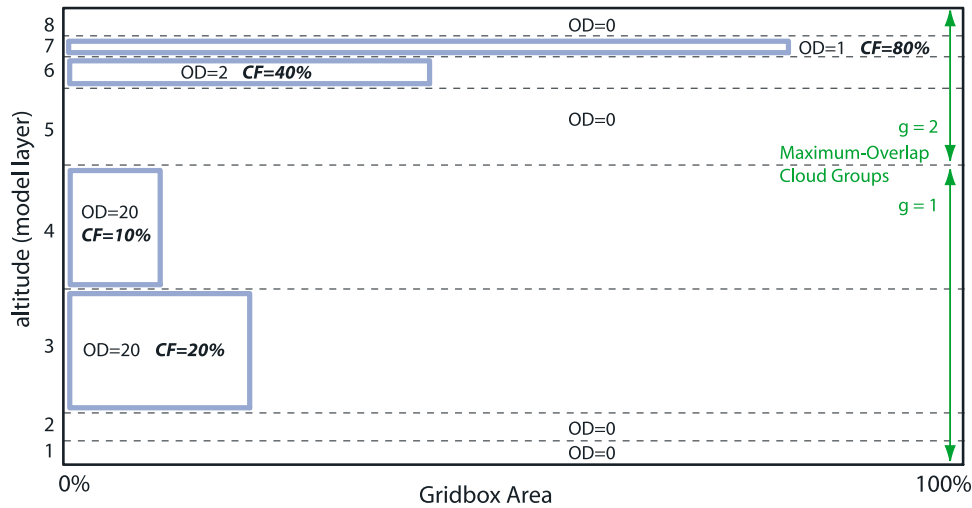


Figure 1. Specification of fractional cloud cover in an idealized grid square in terms of cloud fraction (CF) and optical depth (OD) in each model layer. The clouds (in layers 3, 4, 6, and 7) are assumed to occupy the full vertical extent of the layer but only a fraction of the grid square area. One possible scheme for sorting the clouds into maximum overlap groups results in groups $g = 1$ (layers 1–4) and $g = 2$ (layers 5–8), which are shown here and described further in Figure 3.

with 100% CF, resulting in a single ICA as shown in Figure 2. This method, also known as the “linear” method, is clearly contradicted by observations and produces serious errors in photochemical models [Feng et al., 2004], but it is included here because it is still in current use by many CTMs [e.g., Wild and Prather, 2006].

2.1. Random Overlap

[12] Random overlap adopts the extreme assumption that there is no correlation between clouds in adjacent layers. In this case, the number of ICAs grows exponentially (2^N) with the number of cloudy levels (N). For the example in Figure 1, random overlap would produce 16 ICAs (not shown), still a manageable computation. If all 8 layers had nonzero CF this would grow to 256 ICAs; and for modern

atmospheric models, such as the ECMWF 40-level model with up to 36 cloudy layers in the tropics, the number of ICAs quickly becomes untenable ($\sim 10^{10}$). Random overlap works best when models have several layers that match the typical vertical extent of connected cloud systems. With increasing vertical resolution, the random overlap scheme actually asymptotes to a solution that cloud fraction schemes were introduced to avoid; that is, clouds are effectively spread uniformly over the grid square. Bergman and Rasch [2002] investigate a more realistic cloud overlap scheme that invokes a vertical scale height over which cloud layers become successively decorrelated. This scheme, in which the fraction of a cloud that is randomly overlapped with respect to another is based on the physical separation of layers, avoids the nonsensical asymptote of the random

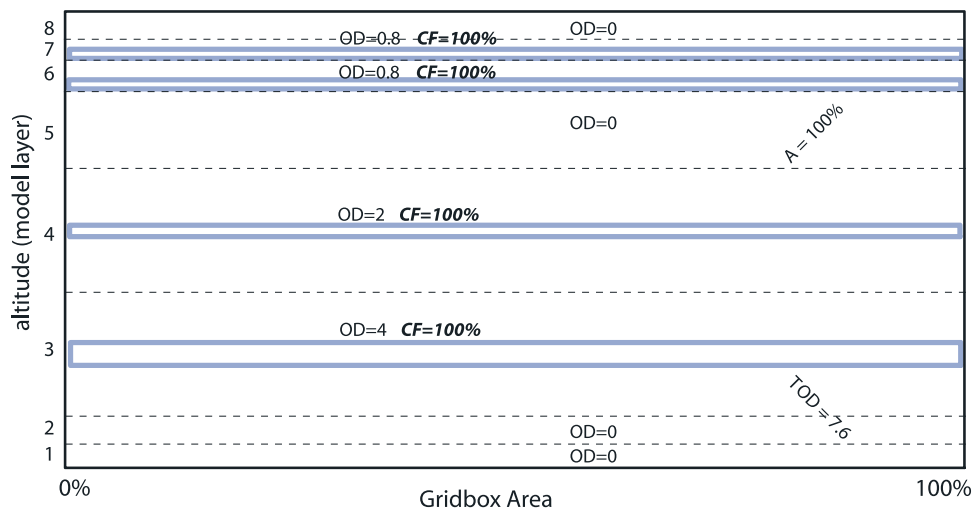


Figure 2. Effective distribution of cloud cover in the idealized grid square of Figure 1 when clouds are averaged (AVG) and only a single column atmosphere (with fractional area (A) = 100% and total optical depth (TOD) = 7.6) is used to calculate J-values (see text).

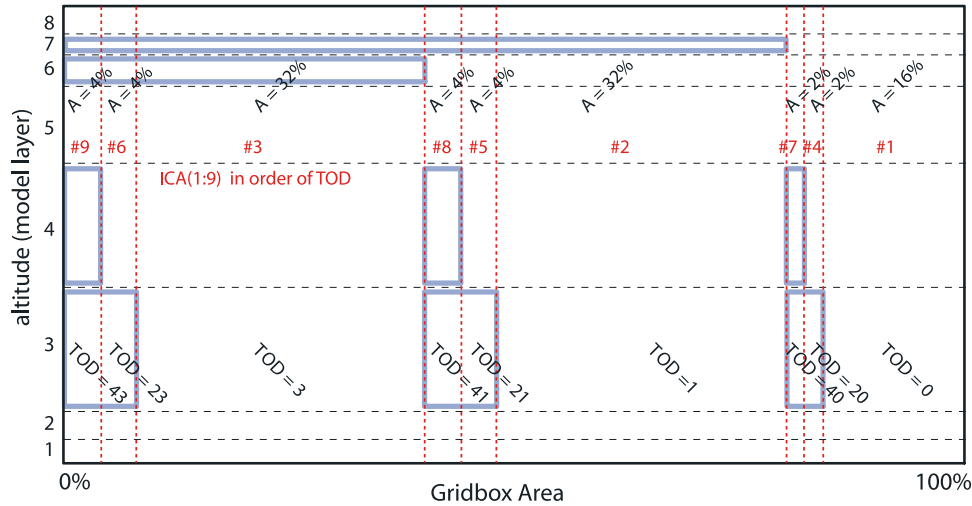


Figure 3. Effective cloud cover for a maximum-random cloud scheme (MXRAN) applied to the two cloud groups for the idealized case in Figure 1. The cloud layers in group 1 (layers 3–4) are maximally overlapped as are those in group 2 (layers 6–7). The two groups are randomly overlapped. Given the CFs in Figure 1, the MXRAN scheme produces nine independent column atmospheres (ICAs), with TOD and fractional area (A) as shown. The ICAs are numbered 1:9 in order of increasing TOD.

scheme as the number of model layers increases. It is still impossible to implement since, as with true random overlap, the number of ICAs grows exponentially with N . We do not attempt to calculate the ICAs and J -values for true random overlap.

[13] *Briegleb* [1992] developed a single ICA approximation for random overlap in which the cloud OD at each level is scaled by the CF, $OD_{\text{RAN}} = OD \times CF^{3/2}$. We include this single ICA approximation, denoted as RAN, in our analysis. This parameterization was developed originally for models with few vertical layers, and may not accurately represent random overlap for the ECMWF 40-level model.

2.2. Maximum-Random Overlap

[14] Maximum overlap of cloud layers, as depicted in Figure 1, produces the minimum number of ICAs for a complex cloudy situation, approaching $N+1$; but observations do not support this scheme. A better alternative, denoted maximum-random (MXRAN), combines the maximum and random overlap assumptions [*Zdunkowski et al.*, 1982; *Collins*, 2001]. In MXRAN, clouds from neighboring levels that are expected to be closely connected are assumed to form a maximum-overlap group. The different groups of clouds are then assumed to be randomly overlapped. Studies show that maximum-random overlap is a reasonable representation of observed cloud distributions over the midlatitude ocean [*Tian and Curry*, 1989], central England [*Hogan and Illingworth*, 2000], the tropical oceans, and midlatitude continental sites [*Mace and Benson-Troth*, 2002], provided that the maximally overlapped clouds are close, within 1 to 2 km in the vertical.

[15] For the CFs shown in Figure 1, if we assume that layers 1–4 form one maximum-overlap group and layers 5–8 form a second, then the MXRAN scheme results in 9 ICAs, which are depicted in Figure 3 with widths proportional to their fractional area (A). The total optical depth ($TOD = \text{sum of all layer OD}$) for each ICA is also shown. In general, the number of ICAs for MXRAN

depends on the grouping, and is given by $(NG_1 + 1) \times (NG_2 + 1) \dots \times (NG_G + 1)$, where NG_g is the number of cloudy levels with unique CF values in group $g = 1:G$. If layers within a maximum-overlap group have the same CF, then they can be treated as a single occurrence in terms of the number of ICAs. Each ICA is identified by a set of indices $(c_{1,n1}, c_{2,n2}, \dots, c_{G,ng})$ where $c_{g,ng}$ corresponds to a specific maximum overlap cloud configuration within each of the cloud groups, $g = 1:G$, with $ng = 1:NG_g + 1$. For the example in Figure 1, $c_{1,1}$ is clear, $c_{1,2}$ has cloud in layer 3, and $c_{1,3}$ has cloud in layers 3 and 4; $c_{2,1}$ is clear, $c_{2,2}$ has cloud in level 7, and $c_{2,3}$ has cloud in levels 6 and 7. The TOD for each ICA is given by the sum of OD in each model layer corresponding to the group indices $(c_{1,n1}, c_{2,n2}, \dots, c_{G,ng})$, and the fractional area A of that ICA is the product of the fractional areas of each of the groups identified by the set of indices. For reasonable choices of the cloud groups, photolysis rates can be calculated for all of the MXRAN ICAs, and compared with the quadrature approximation developed here.

[16] With the MXRAN scheme, the method of grouping clouds must still be determined. We define three different MXRAN schemes as equally plausible, providing a measure of uncertainty in the true answer and some perspective on the errors associated with our quadrature approximation. For the first method, MXRAN-3g, we define three fixed cloud groups by model level to represent the lower (1000–750 hPa), middle (750–350 hPa), and upper (<350 hPa) troposphere [e.g., *Chou et al.*, 1998]. In the second method we form independent groups whenever one or more clear-sky layers separate the cloudy layers [e.g., *Zdunkowski et al.*, 1982]. This method uses a 0% CF threshold to separate groups and is denoted MXRAN-0%. It is the most common form of maximum-random overlap and is found to be consistent with cloud observations [*Collins*, 2001] (see also *Feng et al.* [2004] for discussion of observations of maximum-random versus random). We find, however, that

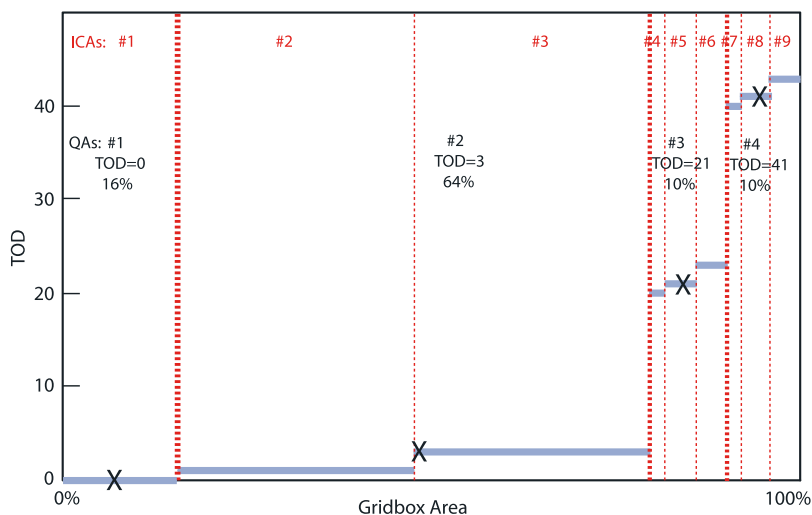


Figure 4. Cumulative probability distribution of TOD versus grid square area for the MXRAN ICAs in Figure 3 (numbered in red at the top of the figure). TOD ranges of 0–1/2 (clear to thin haze), 1/2–4 (cirrus-like), 4–30 (stratus-like), and ≥ 30 (cumulus-like), are used and are marked by thick dashed lines. The ICA in each range selected as the quadrature atmosphere (QA) is marked with a large cross, and its TOD and fractional area are given.

when applying MXRAN-0% to the ECMWF fields in the tropics, middle troposphere cumulus with small CFs and relatively large ODs are often not separated by a clear-sky layer from the cirrus decks above or the stratus below. In order to avoid a single maximally overlapped column, we define a third method in which we use a CF threshold of 8.75% to further separate cloud groups after the initial grouping based on clear-sky layers has been completed. In this method, denoted MXRAN-9%, CF values in the first four nonzero bins (CF = 1.25%, 3.75%, 6.25%, 8.75%, see section 5.2 for description of CF binning) are treated as clear sky layers for the purpose of generating the maximum-overlap groups. These small, but nonzero, CFs are then assigned to the nearest cloud group above or below and included as cloud layers in the photolysis calculations. These three cloud grouping algorithms are intended to demonstrate a range of possibilities. The “correct” method can only be determined by comparing the cloud statistics of a particular model to observations.

2.3. Radiative Transfer

[17] In calculating photolysis rates, we assume that the transmission and scattering of sunlight through a single profile of clouds can be solved exactly by the equations of radiative transfer for a plane-parallel (i.e., horizontally homogeneous) atmosphere, including spherically attenuated solar source terms [Logan *et al.*, 1981] and elastic multiple scattering using the full, forward peaked phase function for the large cloud particles [Wild *et al.*, 2000]. By treating the possible realizations of vertical cloud distribution as a set of independent column atmospheres (ICAs), we implicitly assume that the horizontal scale of homogeneous cloud layers is much greater than the vertical extent (~ 10 km) and thus the radiative transfer can be solved with the plane-parallel assumption. If CTM resolution were to approach the horizontal scales (≤ 10 km) where cloud fraction in a grid could be diagnosed as either 0 or 100%, then the horizontal

and vertical variations would be comparable, and the plane-parallel assumption would have to yield to multidimensional radiative transfer [Di Giuseppe, 2005; Wood *et al.*, 2005; Pincus *et al.*, 2005]. For example, Trautmann *et al.* [1999] looked at idealized 2-D distributions of clouds such as stratus bands and studied how photolysis rates could be averaged.

3. Quadrature Approximation of the Cloud Field

[18] The basis for our method is the assumption that the integration of the radiation field over a large number of ICAs can be approximated by selecting a few representative ICAs, each with an area weighting equal to the sum of the fractional areas of similar ICAs. Our approach is shown schematically in Figures 3 and 4. Figure 3 shows the full set of 9 MXRAN-0% ICAs corresponding to the CFs of Figure 1, each plotted with a width equal to its fractional area in the grid. The sorting of the ICAs(1:9) in order of increasing total optical depth generates the cumulative distribution function for TOD shown in Figure 4.

[19] We now select TOD ranges to determine our quadrature atmospheres, QA(1:4). In this idealized case, as in the calculations using the ECMWF cloud fields (section 5), QA(1) includes $0 \leq \text{TOD} < 1/2$ (clear to thin haze); QA(2), $1/2 \leq \text{TOD} < 4$ (cirrus-like); QA(3), $4 \leq \text{TOD} < 30$ (stratus-like); and QA(4), $30 \leq \text{TOD}$ (cumulus-like). The method used to determine these ranges is discussed in section 5.3. Each quadrature atmosphere has an area equal to the width of its TOD range in the cumulative distribution function as shown in Figure 4, and each is represented by the ICA in the middle of its range. In this example, QA(1) is ICA(1) with TOD = 0 and 16% area coverage; QA(2) is ICA(3) with TOD = 3 and 64% area, QA(3) is ICA(5) with TOD = 21 and 10% area, and QA(4) is ICA(8) with TOD = 41 and 10% area. The number of QAs may be less than 4 if the TOD ranges set above are not represented in a particular

cloud profile, e.g., for nearly clear atmospheres (all TOD < 1/2) there is only one QA.

[20] The use of TOD to sort for similar ICAs is not perfect since there are other degrees of freedom: For example, two columns with clouds of OD = 10 at 200 hPa and 900 hPa, respectively, will have very different profiles of photolysis rates. However, as we shall show in section 5, the small errors found in this quadrature approximation for the ECMWF cloud fields indicate that TOD is, in general, a good selector of ICAs with similar profiles of photolysis rates, though it does not always work well in specific cases with a great deal of vertical structure within one or more TOD ranges.

[21] Note that our quadrature method depends on the MXRAN grouping, as it approximates the average photochemistry for the full set ICAs generated by a specified cloud overlap scheme. In section 5 we calculate average photolysis rates using this approximation for specific MXRAN schemes described in section 2: QUAD-3g is the approximation for the MXRAN-3g scheme; QUAD-0%, for the MXRAN-0% scheme; and QUAD-9%, for the MXRAN-9% scheme. The errors in the quadrature method (i.e., QUAD-3g versus MXRAN-3g) are compared with the differences in cloud overlap schemes (i.e., MXRAN-3g versus MXRAN-0%).

4. Fast-JX

[22] The original fast-J model [Wild *et al.*, 2000] calculated photolysis rates in the troposphere using an asymmetric Feautrier multiple-scattering code that accurately simulated the scattering of clouds and aerosols using their exact optical properties (i.e., single scattering albedo and phase function). Fast-J also optimized the wavelengths longer than 290 nm (all sunlight relevant for tropospheric photochemistry) into 7 bins, and thus it became a practical CTM component for in-line calculation of photolysis rates. Fast-J2 [Bian and Prather, 2002] extended this model to the stratosphere and lower mesosphere by adding 11 wavelength bins from 177 to 290 nm to include all photolysis rates up to 60 km. Fast-J2 dropped the multiple scattering calculation in these wavelengths and calculated the radiation field from simple exponential attenuation of sunlight, an approximation that works well when stratospheric aerosols are at background levels. Without scattering, Fast-J2 could not accurately calculate stratospheric photolysis rates at low sun or in twilight, a serious error for the high-latitude winter stratosphere.

[23] Fast-JX merges the two models. The multiple scattering calculation, with a spherical atmosphere to attenuate the solar beam, is extended to all 18 wavelengths. Fast-JX can thus simulate Pinatubo conditions as well as twilight polar chemistry. An important new feature in fast-JX is the algorithm for adding additional levels to solve the radiative transfer problem in optically thick clouds. In fast-J, maintaining the accuracy of the scattering solution required that within a cloud layer with OD > 1, extra layers of optical thickness no greater than 1 be inserted. This caused large added cost for cumulus clouds of OD greater than 100, which were often found in the GISS met fields. Fast-JX also adds extra layers within a cloudy layer, but uses geometric spacing of successive layers: starting with a very small

optical depth of 0.01 at the top of the uppermost cloud, successive layers increase in optical depth by at most a factor of 1.18. Extensive testing showed that this approximation typically reduced the scattering costs by a factor of 2 to 3 and that scattering errors are much reduced at the top of clouds, less than 0.3% when compared with fully resolved solutions. In terms of coding, fast-JX has been rewritten for parallel computing, with reduced use of common blocks and simplified input data sets. A bug found in the cross-section averaging (R. Uhl and T. Reddman, personal communication, 2005) has been corrected. Other significant improvements include updated solar fluxes based on SUSIM data and cross sections (see web site for current version, <http://www.ess.uci.edu/~prather>).

5. Photolysis Rates for the ECMWF Cloud Fields

[24] Our original CTM modeling with the Oslo-derived ECMWF met fields [Wild *et al.*, 2003] used the AVG approximation with the 3-hourly averaged CFs from the 40-level forecast model, run at T159 and reduced to T63 ($\sim 1.9^\circ$) or T42 ($\sim 2.8^\circ$) resolution. The lowest 5 ECMWF levels, below 200 m, are collapsed into 2 CTM levels, giving us the T42L37 resolution that is used here. Only the lowest 33 levels contain clouds. Comparison with observations [Allan *et al.*, 2004] indicates that errors in outgoing radiation with this generation model (ERA40) appear to be related to inaccurate cloud radiative properties, not the cloud distributions.

[25] Here we use the fast-JX algorithm to calculate the photolysis rates for the different MXRAN schemes. We compute J-values as the average over the full set of MXRAN ICAs and compare them to the average over the approximating QAs. For our T42L37 met-fields, there are often more than a thousand ICAs per grid square in the tropics. The computation of photolysis rates for the full set of MXRAN ICAs is readily done with fast-JX for these one-day tests, but is not feasible for multiyear CTM simulations, and, as we show, is a wasteful approach to derive average J-values.

[26] For the case study here we adopt a monthly zonal mean climatology for ozone (G. Labov, private communication, 2002) [see McPeters *et al.*, 2003] and an aerosol-free atmosphere. The lack of aerosols biases our global mean photolysis rates toward high values [see Bian *et al.*, 2003; Martin *et al.*, 2003] but does not affect our analysis of errors in the representation of fractional cloud cover. Figures 5–8 show the application of our methods to a single grid square (5.6–8.4°N, 23.9–26.7°W) from the 1200–1500 UT 15 January 2000 ECMWF cloud field at a single solar zenith angle, 29.7° (1200Z). Table 1 and Figure 9, discussed in section 5.4, give results for 24-hour integrations for 15 January 2000 (8×3 -hour-average cloud fields, J-values calculated hourly) over different regions of the globe.

5.1. Cloud Optical Properties

[27] The archived meteorological fields provide cloud fraction (CF), cloud liquid water content (LWC, g m^{-3}) and cloud ice water content (IWC, g m^{-3}) for each model level. We determine the optical depth for liquid water as $\text{OD}_w = (\text{LWC}/\text{CF}) (3Q_{\text{ext}}/4\rho R_{\text{eff}}) (\Delta p/\text{g})$. The second factor is derived from the size distribution of cloud droplets: Q_{ext}

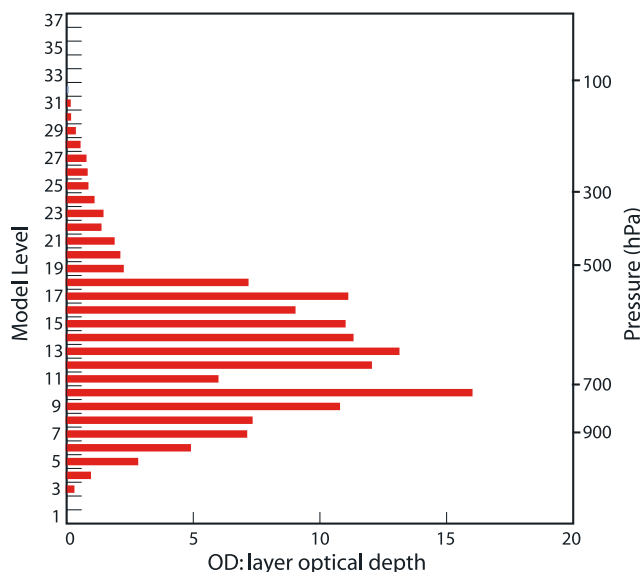


Figure 5. Profile of cloud optical depth (OD) in each model level from a single sample grid square (5.6–8.4°N, 23.9–26.7°W) from the 1200–1500 UT 15 January 2000 ECMWF cloud fields at T42 resolution. Separation between liquid and ice clouds is given, but not shown.

is the extinction efficiency (ratio of extinction cross section to area cross section); R_{eff} is the area-weighted mean droplet radius; and ρ is the density of liquid water (10^6 g m^{-3}). The third factor is the atmospheric mass: Δp is the pressure-thickness of the model layer; and g is the gravitational constant. For ice clouds, the optical depth is parameterized as $OD_i = (IWC/CF) \Delta z / (0.0306 + 0.2548 IWC/CF)$, where Δz is the thickness of the layer [see *Sun and Shine, 1995*]. The cloud optical depth for each layer (Figure 5) is given by $OD = OD_w + OD_i$, but for convenience here the optical properties (single scattering albedo and scattering phase function) are determined solely by the phase with the largest optical depth.

[28] The scattering phase function for liquid clouds is calculated using the UCI Fast-JX Mie algorithm [*Wild et al., 2000*], assuming a Deirmendjian C1 cloud droplet distribution. For levels with mean altitudes less than 1.5 km, we select $R_{\text{eff}} = 9.6 \mu\text{m}$, typical of marine stratus [*Miles et al., 2000*]. For levels above 3.2 km, we fix $R_{\text{eff}} = 12.7 \mu\text{m}$, typical of marine cumulus [*Tampieri and Tomasi, 1976*]. Linear interpolation is used in between. This simplistic approach is adequate for these tests, but accurate CTM simulations will probably need to differentiate between polluted, continental, and clean marine clouds. The scattering phase function for ice depends on temperature, with the phase function for hexagonal crystals used for $T > -40^\circ\text{C}$ and the phase function for irregular crystals used for $T < -40^\circ\text{C}$. These ice-cloud phase functions are approximations to those calculated by M. Mishchenko (personal communication, 2000) and are discussed by *Wild et al. [2000]*.

5.2. Maximum-Random Grouping

[29] CF on the ECMWF T42 grid is archived in increments of 0.78125%. Since the number of ICAs in each maximum overlap group is $NG + 1$, where NG is the

number of nonidentical values of CF, we reduce the number of calculations by binning all nonzero CFs into increments of 2.5%. This gives us CF values of 0%, 1.25% (0.78125–2.34375%), 3.75% (3.125–4.6785%), ... 98.75% (97.65625–100.0%). We use these binned CFs for the purpose of determining the full set of MXRAN ICAs and the fractional areas associated with them, but retain the exact cloud fraction for the calculation of OD. For a typical grid square in the tropics, the binning of CF reduces the number of ICAs by about 40%.

[30] Figure 6 shows the binned CF corresponding to the OD profile in Figure 5, as well as the cloud groups and total number of ICAs resulting from our three MXRAN grouping methods. For this grid square, MXRAN-3g results in 462 ICAs ($7 \times 6 \times 11$), MXRAN-0% gives a single maximally overlapped group with only 15 ICAs, and MXRAN-9% results in 3 groups with 336 ICAs ($7 \times 4 \times 12$). On average, MXRAN-0% yields 32 ICAs per grid square in the tropics, while MXRAN-9% averages 139 ICAs, and MXRAN-3g averages 196 ICAs. The different MXRAN schemes lead to different realizations of the vertical cloud overlap and thus, as shown in sections 5.3 and 5.4, to profiles of J-values that differ on average by a few percent.

5.3. Quadrature Approximation of Photolysis Rates

[31] The cumulative distribution of TOD is shown in Figure 7 for the 15 ICAs of the MXRAN-0% scheme depicted in Figure 6, along with the TOD ranges for determining the QAs (see section 3). For this example, there are 3 ICAs within the clear sky bin, and QA(1), with 38.75% of the area, is represented by ICA(1) with TOD = 0.0.

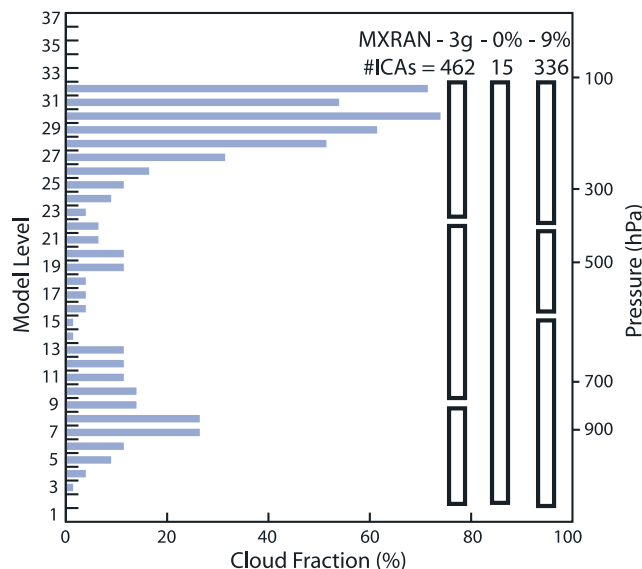


Figure 6. Cloud fraction (CF, %) in each model level for the sample grid square in Figure 5. The vertical black bars show the cloud groupings (maximum overlap within the group, random overlap between groups) for the three different MXRAN schemes. MXRAN-3g has three fixed cloud groupings and generates 462 ICAs; MXRAN-0% has a 0% threshold between groups, which in this example results in only one group and 15 ICAs; and MXRAN-9%, with a 9% threshold, yields three groups and 336 ICAs.

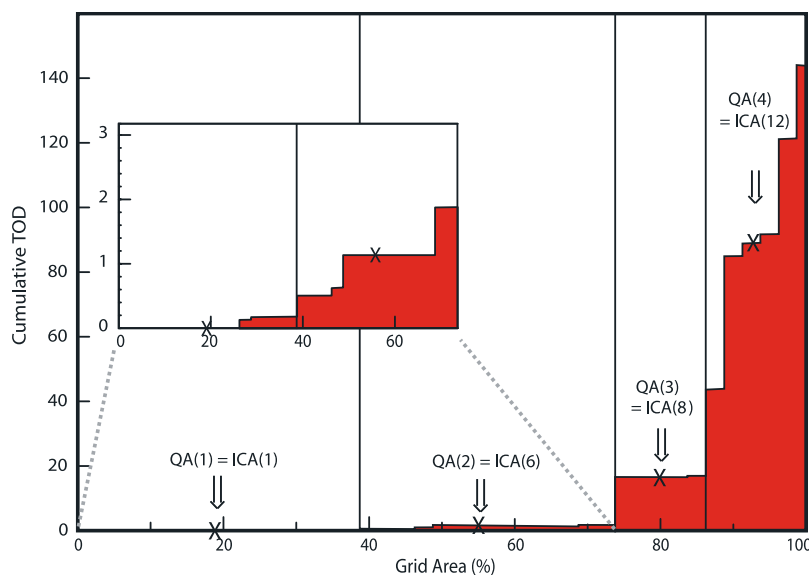


Figure 7. Cumulative total optical depth (TOD) versus grid area (%) for the sample grid square in Figures 5 and 6 using the MXRAN-0% scheme. The TOD ranges for the quadrature scheme adopted in this paper (0–1/2, 1/2–4, 4–30, and ≥ 30) are marked by vertical black lines. The 4 ICAs chosen to be QAs are marked with a large cross. The inset shows a magnified view of the first two TOD ranges.

The other QAs are ICA(6) with TOD = 1.14 and 35.0% weight, ICA(8) with TOD = 16.28 and 12.5% weight, and ICA(12) with TOD = 88.75 and 13.75% weight. The TOD ranges used to locate the 4 QAs were determined by manual adjustment of the quadrature scheme using obvious breakpoints in the probability distribution function of TOD to minimize the errors for the 24-hour-average global J-values (see 5.4 below). The TOD breakpoints (0-1/2-4-30) are fixed for our simulations with these ECMWF fields, but would have to be reexamined for different meteorological fields.

[32] Altitude profiles for the J-values of O_3 (yielding $O(^1D) + O_2$, designated O_3-O^1D), NO_2 , and NO_3 (sum of both $NO + O_2$ and $NO_2 + O$ pathways) are shown for the sample grid square in Figure 8. These three J-values exhibit

different sensitivities to the three basic radiative processes controlling photochemistry: scattering by clouds and aerosols (O_3-O^1D , NO_2 , NO_3), Rayleigh scattering (O_3-O^1D , NO_2), and ozone absorption (O_3-O^1D). The J-value profiles for the three MXRAN grouping methods, 3g (cyan), 9% (magenta), and 0% (black), are shown as solid colored lines along with profiles for QUAD-0% (approximation to MXRAN-0%, very thick black dashed) and the RAN (black dashed) and AVG (grey dashed) schemes. There is some variation between the three MXRAN solutions. Note that the -3g and -9% schemes have more structure in the middle troposphere than the -0%, which has only 1 cloud grouping. The AVG photolysis rates are much larger than the MXRAN rates in the free troposphere and much smaller

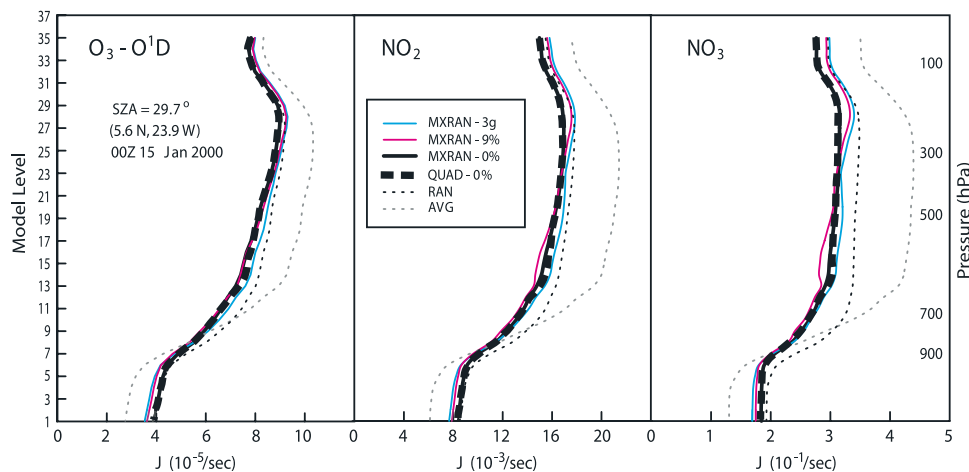


Figure 8. J-value profiles versus model level for the sample grid square described in Figures 5–7 at 1200Z (solar zenith angle = 29.7°). J-values (s^{-1}) are shown for (left) O_3-O^1D , (middle) NO_2 , and (right) NO_3 ; see text. Exact J-values using all ICAs are shown for MXRAN-3g (cyan solid), -9% (magenta solid), and -0% (thick black solid line). The QUAD-0% (very thick black dashed), as well as the RAN (black dashed) and AVG (grey dashed), approximations are also shown.

Table 1. Root Mean Square Errors (%) in the 24-Hour Average J-Values of O₃-O¹D, NO₂, and NO₃^a

	Group Difference 3-0%	Group Difference 9-0%	QUAD Error 3g	QUAD Error 9%	QUAD Error 0%	RAN Error	AVG Error
<i>Tropics</i>							
O ₃ -O ¹ D	2.6	0.9	3.1	2.2	1.5	5.2	12.8
NO ₂	3.0	1.1	3.0	2.1	1.4	6.5	15.7
NO ₃	3.7	1.4	3.2	2.3	1.6	10.7	21.2
<i>Midlatitudes</i>							
O ₃ -O ¹ D	1.1	0.2	2.4	1.6	1.4	2.1	4.6
NO ₂	1.6	0.3	2.6	1.8	1.6	3.1	6.5
NO ₃	2.3	0.4	3.2	2.3	2.1	6.1	10.4
<i>Northern High Latitudes</i>							
O ₃ -O ¹ D	0.2	0.0	0.9	0.6	0.6	0.5	0.6
NO ₂	0.4	0.1	1.7	1.3	1.2	0.9	1.4
NO ₃	3.1	0.5	7.7	6.6	6.2	9.0	12.4
<i>Southern High Latitudes</i>							
O ₃ -O ¹ D	0.2	0.0	0.7	0.5	0.4	0.5	0.8
NO ₂	0.4	0.1	0.8	0.5	0.5	0.6	1.3
NO ₃	0.8	0.1	1.1	0.8	0.7	1.3	2.5

^aThe errors are weighted using the pressure thickness of each layer in the vertical, and they are averaged over the tropics (30°S–30°N), midlatitudes (60–30°S plus 30–60°N), and the northern and southern high latitudes (90–60°S and 60–77°N). Columns 2 and 3 give the difference between the MXRAN schemes: 3g minus 0%, and 9% minus 0%. Columns 4–6 give the error for the QUAD approximation to each MXRAN grouping scheme. Columns 7–8 give the error for the RAN and AVG schemes relative to MXRAN-0%.

in the boundary layer. The RAN photolysis rates are somewhat larger than the MXRAN rates throughout the troposphere in this particular example. Most importantly, the QUAD-0% J-values closely match those of MXRAN-0%. Results are similar (not shown) for QUAD-9% and MXRAN-9%, and for QUAD-3g and MXRAN-3g.

5.4. Global Errors in Photolysis Rates

[33] A more rigorous evaluation of the accuracy of the quadrature method is provided by 24-hour integration of J-values over all of the grid squares (128 longitude × 64 latitude) in the T42L37 met fields. We compute the J-values for each grid square beginning at 1200Z on 15 January 2000. The solar zenith angle is updated every hour, and the cloud fields are read in every 3 hours. The 24-hour-averaged J-values for O₃-O¹D, NO₂, and NO₃ are stored at each model level in each grid square for all of the MXRAN and QUAD schemes, as well as RAN and AVG. For each grid square we then calculate a root-mean-square (rms) difference (in %) between two schemes using the pressure thickness of each model layer for vertical weighting. This is averaged for four regions: tropics (30°S–30°N), midlatitudes (60–30°S plus 30–60°N), and northern and southern high latitudes, excluding the dark winter pole (90–60°S and 60–77°N, separately). In addition to the RMS difference (Table 1), we also include a similarly calculated mean error (bias) in the boundary layer (defined as model levels 1–8, typically below 1000 m height) and in the free troposphere (model levels 14–37). These bias errors are shown in Figure 9.

[34] As seen in Table 1, the RMS error in the quadrature approximation (computed for MXRAN-3g, for example, as the pressure-weighted average of

$\sqrt{(\text{QUAD-3g} - \text{MXRAN-3g})^2 / \text{MXRAN-3g}}$), is small, generally less than 3%, except for J-NO₃ in northern (winter) high latitudes (see later discussion). Typically, these errors are comparable to or smaller than the difference between the MXRAN-3g and -0% schemes; that is, the quadrature error is less than the uncertainty in our cloud groupings. The biases generated by the QUAD approximation (Figure 9) are negligible (<1%) in both the boundary layer and free troposphere, and are again less than the differences between MXRAN schemes.

[35] In contrast, the J-values using the AVG and RAN approximations differ greatly from those of a maximum-random overlap scheme and lead to large errors in the chemistry as demonstrated by Feng *et al.* [2004]. The RMS errors are typically 12–21% for AVG and 5–11%

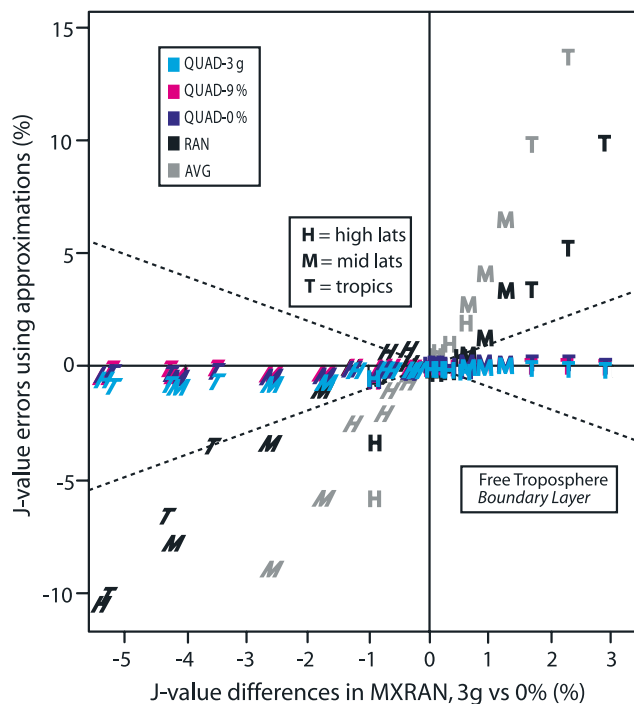


Figure 9. J-value relative errors (%) of the quadrature approximation to each of the three different MXRAN schemes are plotted against the corresponding J-value relative differences (%) between two MXRAN schemes (3g minus 0%). Errors are computed for the 24-hour average J-values of O₃-O¹D, NO₂, and NO₃ at each grid square and each model level for the 15 January 2000 ECMWF fields (T42 resolution). Errors are then averaged over latitude belts (H, high latitudes north and south (separately); M, midlatitudes; T, tropics) and over model level (roman indicates free troposphere, levels 14–37; italics indicate boundary layer, levels 1–8). The errors in the quadrature approximation for each MXRAN scheme are color coded (cyan indicates QUAD-3g, magenta indicates QUAD-9%, and dark blue indicates QUAD-0%), but are not all visible as they tend to cluster along the abscissa. The errors in the RAN (black) and AVG (gray) approximations are calculated relative to MXRAN-0%. Errors bounded by the 1:1 dotted lines are smaller than the difference between alternate MXRAN schemes. AVG scheme errors in the tropics greater than 15% are not shown.

Table 2. Modified Shortwave Albedo (290–850 nm) in % Using Fast-JX for the Same 24-Hour Period and Latitude Ranges as Table 1^a

	UV-VIS Albedo, %		Absolute Error, %		
	MXRAN-3g	MXRAN-0%	QUAD-0%	RAN	AVG
Tropics	39	35	+0.0	+7.6	+18.7
Midlatitudes	47	45	+0.1	+2.8	+7.8
Northern high latitudes	66	66	+0.2	+1.0	+2.2
Southern high latitudes	29	29	−0.1	−0.4	+1.6

^aColumns 2 and 3 give the albedo for the MXRAN-3g and -0% cloud overlap schemes. Columns 4–6 give the absolute errors in the albedo for the QUAD-0%, RAN, and AVG schemes relative to MXRAN-0%.

for RAN in the tropics and subtropics where most chemical production and loss occurs. In the tropical boundary layer, the AVG photolysis rates are typically 20% smaller than the MXRAN rates, while the RAN photolysis rates are 3–10% smaller. In the free troposphere, both approximations overestimate the J-values.

[36] One key assumption of the quadrature method is that ICAs with similar TOD will have similar photolysis rate profiles, so that choosing representative ICAs based on TOD will result in nearly the same average profile as using the full set of ICAs. This assumption breaks down somewhat in the calculation of NO₃ photolysis rates in the winter high latitudes (i.e., there are 6–8% RMS errors with QUAD). Because high-latitude, high-altitude clouds are often optically thin, many ICAs are represented by a single QA. At large solar zenith angles, however, each ICA is effectively opaque to transmission of the direct solar beam. At long wavelengths, where NO₃ is photolyzed, there is little Rayleigh scattering of sunlight above these clouds, and J-NO₃ is effectively zero below cloud top. A single QA cannot accurately represent the attenuation of J-NO₃ through the different cloud tops of the ICAs. It is difficult to find a simple remedy for this situation, and we can only note that these errors probably have little impact on the photochemistry.

6. Discussion and Implications

[37] This approach has implications that extend beyond the calculation of photolysis rates. For example, the shortwave albedo, a key component of the energy budget, is very sensitive to the choice of cloud overlap scheme. For the 15 January 2000 ECMWF cloud fields, we calculate a modified shortwave (290–850 nm) albedo using fast-JX with the different cloud schemes assuming a Lambertian surface albedo of 0.10. As shown in Table 2, there are important differences in albedo of order 3–4% between the MXRAN-3g and MXRAN-0% schemes, indicating that for consistency, the cloud overlap scheme should match that of the atmospheric model. The albedo error in the quadrature approximation (QUAD-0% minus MXRAN-0%) is less than 0.2%, demonstrating that the quadrature approximation can be used in the atmospheric model to calculate the shortwave heating rates. With fast-JX, there is the additional advantage of automatically including O₃ and aerosols. The albedo error with the AVG and RAN schemes is large, and both methods reflect far too much sunlight from the tropics using the ECMWF cloud fields.

[38] With the quadrature approximation, we can model the subgrid-scale variations in atmospheric chemistry associated with clouds. As an example, we repeat the Marine case study of the IPCC PhotoComp [Prather *et al.*, 1995;

Olson *et al.*, 1997]. We select the cloud parameters from our sample grid square (Figures 5 and 6) and precalculate the J-values for each of the four QUAD-0% QAs in the lowest T42L37 model level ($z = 20$ m). Using the J-values for the four QAs as well as the weighted average, we integrate our photochemical box model for 5 days, initializing with the PhotoComp specifications for the marine boundary layer (O₃ = 30 ppb). Photolysis of O₃ and reaction of O(¹D) with H₂O result in a steady loss of O₃ over the 5-day period that is most rapid about noon. As shown in Figure 10, the clear sky QA (bottom curve) has the greatest loss of boundary layer O₃, while the cloudiest QA (top curve) has the least. We compare the noontime O₃ calculated from the weighted average of these four separate atmospheres with that calculated in a single atmosphere using the average J-values (also shown in Figure 10). The results from averaging the separate photochemistries do not differ noticeably from the results of a single photochemistry with

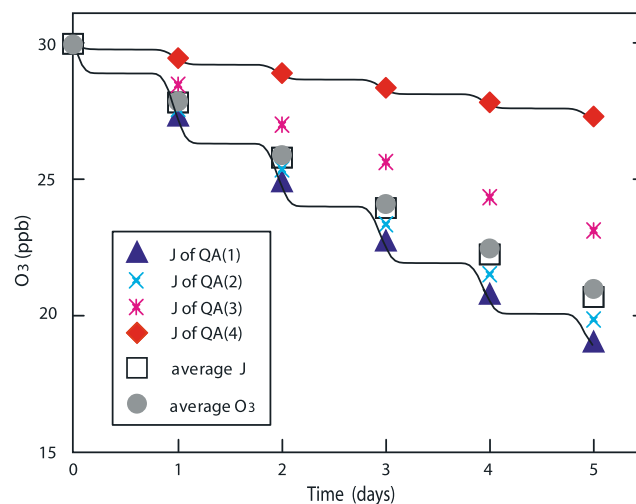


Figure 10. Five-day integration of O₃ (ppb) starting at noon in accord with the PhotoComp marine boundary layer protocol (see text). Atmospheric profiles (T, O₃, clouds) are taken from the example grid square (Figures 5–8). The loss of O₃ is integrated separately in the lowest level of each of the four QAs from Figure 7. Noon values are shown in order of increasing TOD as dark blue triangles, cyan crosses, magenta asterisks, and red diamonds. A single atmosphere integrated with the grid-average J-values is shown as open squares and can be compared with the gray solid circles, which represent the area-weighted average of O₃ from the four separate QA integrations. The continuous lines show the hourly loss of O₃ for clear sky (bottom, QA(1)) and the most cloudy conditions (top, QA(4)).

the average J-values. One can see that the results would be similar if we had chosen to remix the fractional volumes every hour instead of at the end of 5 days. For comparison, using the AVG approximation would have led to 20% less ozone loss over the 5 day period.

[39] This particular example is overly simplistic since we restricted the test to gas phase chemistry and thus did not invoke heterogeneous chemistry within the cloudy fraction. There is no clear formalism for treating subgrid differences in chemistry within a single grid box without fully resolving the problem (i.e., specifying separate cloudy versus clear initial conditions as well as the transport between the subgrid volumes). Nevertheless, we propose that extending the quadrature atmosphere approach to heterogeneous cloud chemistry, but mixing and reinitializing the trace species every 1/2 to 2 hours, will provide a good approximation of this complex chemistry as long as the change in abundance of the key chemical constituents over this mixing time is still in a linear regime (i.e., much less than one e-fold). The treatment of highly nonlinear chemistry acting on short timescales with respect to the lifetime of the clouds, e.g., the reaction of H₂O₂ and SO₂ in cloud droplets, will require further testing.

[40] We have shown that photolysis rates for maximum-random cloud distributions can be averaged accurately using a subset of only four cloud profiles, selected on the basis of total cloud optical depth. Our method provides a powerful tool for representing the effects of complex cloud distributions on photochemistry at modest computational cost. It can be readily implemented in CTMs or any atmospheric model, it can be chosen to be consistent with the cloud statistics of the underlying atmospheric model or observations, and it avoids the large systematic biases of the currently used single-profile methods. For the ECMWF T42L37 cloud fields tested here, the different MXRAN schemes gave similar J-values and were all equally tractable within a CTM. Some caution is needed in implementing certain MXRAN algorithms since the perverse case of alternating clear and cloudy layers, if encountered, may result in an excessive number of random overlaps ($\sim 10^5$). With this caution, the MXRAN cloud groupings can readily define a probability distribution of total optical depth that can be tested in part with satellite observations. Cloud statistics from other models may in fact contain additional information about cloud connectivity, which would reduce the uncertainty in applying the method. We are currently testing the impact of this improved cloud treatment on tropospheric photochemistry using the UCI CTM, and we will eventually expand the method to include subgrid inhomogeneities in the chemical environment inside and outside of clouds.

[41] **Acknowledgments.** This research was supported by the Comer Foundation and by NASA Global Modeling Initiative grants to the University of California, Irvine, and the University of Michigan.

References

- Allan, R. P., M. A. Ringer, J. A. Pamment, and A. Slingo (2004), Simulation of the Earth's radiation budget by the European centre for Medium-Range Weather Forecasts 40-year reanalysis (ERA40), *J. Geophys. Res.*, *109*, D18107, doi:10.1029/2004JD004816.
- Bergman, J. W., and P. J. Rasch (2002), Parameterizing vertically coherent cloud distributions, *J. Atmos. Sci.*, *59*, 2165–2182.
- Bey, I., D. J. Jacob, J. A. Logan, and R. M. Yantosca (2001), Asian chemical outflow to the Pacific: Origins, pathways and budgets, *J. Geophys. Res.*, *106*, 23,097–23,114.
- Bian, H., and M. J. Prather (2002), Fast-J2: Accurate simulation of stratospheric photolysis in global chemical models, *J. Atmos. Chem.*, *41*, 281–296.
- Bian, H., M. J. Prather, and T. Takemura (2003), Tropospheric aerosol impacts on trace gas budgets through photolysis, *J. Geophys. Res.*, *108*(D8), 4242, doi:10.1029/2002JD002743.
- Briegleb, B. P. (1992), Delta-Eddington approximation for solar radiation in the NCAR community climate model, *J. Geophys. Res.*, *97*, 7603–7612.
- Brooks, M. E., R. J. Hogan, and A. J. Illingworth (2005), Parameterizing the difference in cloud fraction defined by area and by volume as observed with radar and lidar, *J. Atmos. Sci.*, *62*, 2248–2260.
- Chang, J. S., R. A. Brost, I. S. A. Isaksen, S. Madronich, P. Middleton, W. R. Stockwell, and C. J. Walcek (1987), A three-dimensional Eulerian acid deposition model: Physical concepts and formulation, *J. Geophys. Res.*, *92*, 14,681–14,700.
- Chou, M.-D., M. J. Suarez, C.-H. Ho, M. M.-H. Yan, and K.-T. Lee (1998), Parameterization of cloud overlapping and shortwave single-scattering properties for use in general circulation and cloud ensemble models, *J. Clim.*, *11*, 202–214.
- Collins, W. D. (2001), Parameterization of generalized cloud overlap for radiative calculations in general circulation models, *J. Atmos. Sci.*, *58*, 3224–3242.
- Cornet, C., J. C. Buriez, J. Riedi, H. Isaka, and B. Guillemet (2005), Case study of inhomogeneous cloud parameter retrieval from MODIS data, *Geophys. Res. Lett.*, *32*, L13807, doi:10.1029/2005GL022791.
- Di Giuseppe, F. (2005), Sensitivity of one-dimensional radiative biases to vertical cloud-structure assumptions: Validation with aircraft data, *Q. J. R. Meteorol. Soc.*, *131*(608), 1655–1676.
- Faure, T., H. Isaka, and B. Guillemet (2001), Neural network retrieval of cloud parameters of inhomogeneous and fractional clouds—Feasibility study, *Remote Sens. Environ.*, *77*(2), 123–138.
- Feng, Y., J. E. Penner, S. Sillman, and X. Liu (2004), Effects of cloud overlap in photochemical models, *J. Geophys. Res.*, *109*, D04310, doi:10.1029/2003JD004040.
- Gordon, N. D., J. R. Norris, C. P. Weaver, and S. A. Klein (2005), Cluster analysis of cloud regimes and characteristic dynamics of midlatitude synoptic systems in observations and a model, *J. Geophys. Res.*, *110*, D15S17, doi:10.1029/2004JD005027.
- Hogan, R. J., and A. J. Illingworth (2000), Deriving cloud statistics from radar, *Q. J. R. Meteorol. Soc.*, *126*(569), 2903–2909.
- Kylling, A., et al. (2005), Spectral actinic flux in the lower troposphere: measurement and 1-D simulations for cloudless, broken cloud and overcast situations, *Atmos. Chem. Phys.*, *5*, 1975–1997.
- Landgraf, J., and P. J. Crutzen (1998), An efficient method for online calculations of photolysis and heating rates, *J. Atmos. Sci.*, *55*, 863–878.
- Lewis, G. M., P. H. Austin, and M. Szczodrak (2004), Spatial statistics of marine boundary layer clouds, *J. Geophys. Res.*, *109*, D04104, doi:10.1029/2003JD003742.
- Logan, J. A., M. J. Prather, S. C. Wofsy, and M. B. McElroy (1981), Tropospheric chemistry: A global perspective, *J. Geophys. Res.*, *86*, 7210–7254.
- London, J. (1952), The distribution of radiational temperature change in the Northern Hemisphere during March, *J. Meteorol.*, *9*, 145–151.
- Mace, G. G., and S. Benson-Troth (2002), Cloud-layer overlap characteristics derived from long-term cloud radar data, *J. Clim.*, *15*, 2505–2515.
- Madronich, S. (1987), Photodissociation in the atmosphere: 1. Actinic flux and the effects of ground reflections and clouds, *J. Geophys. Res.*, *92*, 9740–9752.
- Martin, R. V., D. J. Jacob, R. M. Yantosca, M. Chin, and P. Ginoux (2003), Global and regional decreases in tropospheric oxidants from photochemical effects of aerosols, *J. Geophys. Res.*, *108*(D3), 4097, doi:10.1029/2002JD002622.
- McPeters, R. D., J. A. Logan, and G. J. Labow (2003), Ozone climatological profiles for Version 8 TOMS and SBUV retrievals, *Eos Trans. AGU*, *84*(46), Fall Meet. Suppl., Abstract A21D-0998.
- Miles, N. L., J. Verlinde, and E. E. Clothiaux (2000), Cloud droplet size distributions in low-level stratiform clouds, *J. Atmos. Sci.*, *57*, 295–311.
- Olson, J., et al. (1997), Results from the IPCC photochemical model inter-comparison (PhotoComp), *J. Geophys. Res.*, *102*, 5979–5991.
- Palm, S. P., A. Benedetti, and J. Spinhirne (2005), Validation of ECMWF global forecast model parameters using GLAS atmospheric channel measurements, *Geophys. Res. Lett.*, *32*, L22S09, doi:10.1029/2005GL023535.
- Pincus, R., C. Hannay, and K. F. Evans (2005), The accuracy of determining three-dimensional radiative transfer effects in cumulus clouds using ground-based profiling instruments, *J. Atmos. Sci.*, *62*(7), 2284–2293.

- Prather, M., R. Derwent, D. Ehhalt, P. Fraser, E. Sanhueza, and X. Zhou (1995), Other trace gases and atmospheric chemistry, in *Climate Change 1994, Intergovernmental Panel on Climate Change*, edited by J. T. Houghton et al., chap. 2, pp 73–126, Cambridge Univ. Press, Cambridge, U. K.
- Spivakovsky, C. M., et al. (2000), Three-dimensional climatological distribution of tropospheric OH: Update and evaluation, *J. Geophys. Res.*, *105*, 8931–8980.
- Sun, Z., and K. P. Shine (1995), Parameterization of ice cloud radiative properties and its application to the potential climatic importance of mixed-phase clouds, *J. Clim.*, *8*, 1874–1888.
- Tampieri, F., and C. Tomasi (1976), Size distribution models of fog and cloud droplets in terms of the modified gamma function, *Tellus*, *28*, 333–347.
- Tian, L., and J. Curry (1989), Cloud overlap statistics, *J. Geophys. Res.*, *94*, 9925–9936.
- Tie, X. X., S. Madronich, S. Walters, R. Y. Zhang, P. Rasch, and W. Collins (2003), Effect of clouds on photolysis and oxidants in the troposphere, *J. Geophys. Res.*, *108*(D20), 4642, doi:10.1029/2003JD003659.
- Trautmann, T., I. Podgorny, J. Landgraf, and P. J. Crutzen (1999), Actinic fluxes and photodissociation coefficients in cloud fields embedded in realistic atmospheres, *J. Geophys. Res.*, *104*, 30,173–30,192.
- Weare, B. C. (1999), Combined satellite- and surface-based observations of clouds, *J. Clim.*, *12*, 897–913.
- Wild, O., and M. J. Prather (2006), Global tropospheric ozone modeling: Quantifying errors due to grid resolution, *J. Geophys. Res.*, *111*, D11305, doi:10.1029/2005JD006605.
- Wild, O., X. Zhu, and M. J. Prather (2000), Fast-J: Accurate simulation of in- and below-cloud photolysis in tropospheric chemical models, *J. Atmos. Chem.*, *37*, 245–282.
- Wild, O., J. K. Sundet, M. J. Prather, I. S. A. Isaksen, H. Akimoto, E. V. Browell, and S. J. Oltmans (2003), Chemical transport model ozone simulations for spring 2001 over the western Pacific: Comparisons with TRACE-P lidar, ozonesondes, and Total Ozone Mapping Spectrometer columns, *J. Geophys. Res.*, *108*(D21), 8826, doi:10.1029/2002JD003283.
- Willen, U., S. Crewell, H. K. Baltink, and O. Sievers (2005), Assessing model predicted vertical cloud structure and cloud overlap with radar and lidar ceilometer observations for the Baltex Bridge Campaign of CLIWNET, *Atmos. Res.*, *75*(3), 227–255.
- Wood, N. B., P. M. Gabriel, and G. L. Stephens (2005), An assessment of the parameterization of subgrid-scale cloud effects on radiative transfer. Part II: Horizontal inhomogeneity, *J. Atmos. Sci.*, *62*, 2895–2909.
- Zdunkowski, W. G., W.-G. Panhans, R. M. Welch, and G. Korb (1982), A radiation scheme for circulation and climate models, *Contrib. Atmos. Phys.*, *55*, 215–238.

J. L. Neu and M. J. Prather, Department of Earth System Science, University of California, 2101 Croul Hall, Irvine, CA 92697, USA. (jne@uci.edu)

J. E. Penner, Department of Atmospheric, Oceanic, and Space Sciences, University of Michigan, 1521C Space Research Building, Ann Arbor, MI 48109-1349, USA.